

Article

An Optimization Algorithm for Embedded Raspberry Pi Pico Controllers for Solar Tree Systems

K. Punitha ¹, Akhlaqur Rahman ², A. S. Radhamani ³, Ramakrishna S. S. Nuvvula ^{4,*}, Sk. A. Shezan ^{2,*}, Syed Riyaz Ahammed ⁵, Polamarasetty P. Kumar ⁶ and Md Fatin Ishraque ⁷

- ¹ Department of Electrical and Electronics Engineering, P. S. R. Engineering College, Sivakasi 626140, Tamil Nadu, India; kgpunitha@gmail.com
- ² Department of Electrical Engineering and Industrial Automation, Engineering Institute of Technology, Melbourne Campus, Melbourne, VIC 3000, Australia; akhlaqur.rahman@eit.edu.au
- ³ Department of Electronics and Communication Engineering, Amrita School of Computing, Amrita Vishwa Vidyapeetham, Nagercoil 629901, Tamil Nadu, India; asradhamani@gmail.com
- ⁴ Department of Electrical and Electronics Engineering, NMAM Institute of Technology, NITTE (Deemed to be University), Karkala 574110, Karnataka, India
- ⁵ Department of Electronics & Communication Engineering, NMAM Institute of Technology, NITTE (Deemed to be University), Karkala 574110, Karnataka, India; syedriyaz.global@gmail.com
- ⁶ Department of Electrical and Electronics Engineering, GMR Institute of Technology, Razam 532127, Andhra Pradesh, India; prvnkumar343@gmail.com
- ⁷ Department of Electrical, Electronics and Communication Engineering, Pabna University of Science and Technology, Pabna 6600, Bangladesh; fatineeruet@gmail.com
- * Correspondence: ramakrishna.n@nitte.edu.in (R.S.S.N.); shezan.arafin@eit.edu.au (S.A.S.)

Abstract: Solar photovoltaic (PV) systems stand out as a promising solution for generating clean, carbon-free energy. However, traditional solar panel installations often require extensive land resources, which could become scarce as the population grows. To address this challenge, innovative approaches are needed to maximize solar power generation within limited spaces. One promising concept involves the development of biological tree-like structures housing solar panels. These “solar trees” mimic the arrangement of branches and leaves found in natural trees, following patterns akin to phyllotaxy, which correlates with the Fibonacci sequence and golden ratio. By adopting an alternative 1:3 phyllotaxy pattern, three solar panels can be efficiently arranged along the stem of the solar tree structure, each rotated at a 120-degree displacement. Optimizing the performance of solar trees requires effective maximum power point tracking (MPPT), a crucial process for extracting the maximum available power from solar panels to enhance the overall efficiency. In this study, a novel metaheuristic algorithm called horse herd optimization (HHO) is employed for MPPT in solar tree applications. Moreover, to efficiently manage the generated power, a cascaded buck–boost converter is utilized. This converter is capable of adjusting the DC voltage levels to match the system requirements within a single topology. The algorithm is implemented using MATLAB and embedded within a Raspberry Pi Pico controller, which facilitates the generation of pulse-width modulation (PWM) signals to control the cascaded buck–boost converter. Through extensive validation, this study confirms the effectiveness of the proposed HHO algorithm integrated into the Raspberry Pi Pico controller for optimizing solar trees under various shading conditions. In essence, this research highlights the potential of solar tree structures coupled with advanced MPPT algorithms and power management systems to maximize solar energy utilization, offering a sustainable solution for clean energy generation within limited land resources.

Keywords: solar tree; Raspberry Pi Pico; horse herd optimization (HHO); metaheuristic algorithm; cascaded buck–boost converter; maximum power point tracking (MPPT)



Citation: Punitha, K.; Rahman, A.; Radhamani, A.S.; Nuvvula, R.S.S.; Shezan, S.A.; Ahammed, S.R.; Kumar, P.P.; Ishraque, M.F. An Optimization Algorithm for Embedded Raspberry Pi Pico Controllers for Solar Tree Systems. *Sustainability* **2024**, *16*, 3788. <https://doi.org/10.3390/su16093788>

Academic Editors: Jian Zhang, Heejin Cho and Dongsu Kim

Received: 20 February 2024

Revised: 17 March 2024

Accepted: 22 April 2024

Published: 30 April 2024



Copyright: © 2024 by the authors. Licensee MDPI, Basel, Switzerland. This article is an open access article distributed under the terms and conditions of the Creative Commons Attribution (CC BY) license (<https://creativecommons.org/licenses/by/4.0/>).

1. Introduction

As some of the most significant options, solar irradiance systems with photovoltaic panels can harness the sun as an energy source to be turned into electrical power. Since it has several benefits, including not requiring any fuel expenditure, not harming the environment, requiring little maintenance, and producing no noise, photovoltaic (PV) energy is becoming more and more significant as a renewable energy source. PV energy conversion is based on the generation of electric currents from light absorption by semiconductor materials. However, the efficiency and stability of PV devices are still limited by various factors, such as material defects, environmental conditions, and device architectures [1–4]. The installation of conventional solar panels requires a considerable land area, which will become less available as the population increases. The aforementioned issues can be resolved by designing biological tree-like structures to maximize the solar power output over a small area of land. To maximize the output power from solar panels, three-dimensional arrangement strategies have been proposed [5]. Natural trees' branches and leaves follow a particular pattern known as phyllotaxy, which is directly comparable to the Fibonacci sequence and golden ratio, serving as a common source of inspiration for the arrangement of such panels. The solar tree approach is a novel design for solar photovoltaic systems that mimics the structure of a tree to save space and increase efficiency. The real-world applications of this unique solar tree system include mounting several solar panels to a single pillar, resulting in a tree-like structure that uses sunlight to generate direct current (DC) from solar power. The tree structure enhances the architectural appeal while also addressing land urbanization concerns. Such a system may power streetlights, decreasing reliance on the grid; serve as a charging station for electric vehicles; and improve the visual attractiveness of outdoor settings, among other things. Off-grid installations enable solar trees to run independently and deliver dependable power, even in remote locations. However, solar tree systems face the challenge of extracting the maximum power from the solar panels under varying environmental conditions. Several studies have explored the design and implementation of solar trees, emphasizing their aesthetic appeal, space efficiency, and potential for harvesting urban energy. In [6], under equivalent irradiation conditions, the power generation rates of two different phyllotaxy arrangements of solar trees were compared. There are numerous different phyllotaxy patterns, including 1:3, 2:5, and 3:8. The orientation direction of solar panels is distinct when they are positioned in different phyllotaxy patterns [7]. In contrast to traditional panels, which are oriented unidirectionally, solar trees house solar panels connected in various directions, allowing them to gather more sunshine throughout the day.

To obtain the maximum possible conversion rate of electricity from solar panels, maximum power point tracking (MPPT) can be utilized. MPPT involves continuously changing the angle of panels in line with the change in the angle of sunlight. However, these tracking operations require some electricity to power the tracking equipment. Hence, the utilization of the best MPPT algorithm is the optimum way to exact the maximum available power from the solar panels. Regarding the nonlinear I-V-P-V characteristics and the current I , which depend on the sunlight, solar temperature, and load settings, solar PV systems typically have comparatively low conversion efficiency rates [8]. As a result, the system, which transfers power from the solar PV array to the load, must operate at the maximum available power rate. A solar PV system typically contains two converter stages, one for a DC–DC converter and the other for a DC–AC converter. The initial stage must regulate variations in the solar PV system's output maximum power point [9]. In other words, the maximum power point tracking process is controlled by modulating the duty ratio of the DC–DC converter [10]. Many MPPT methods such as conventional and soft computing methods are mentioned in the literature to control DC–DC converters to provide maximum power. However, the conventional methods have some disadvantages regarding the oscillations around the MPP, while the soft computing methods take more time to reach the MPP and its high implementation cost. Existing methods of maximum power point tracking (MPPT) are either too slow, too complex, or too oscillatory to achieve

optimal performance. Therefore, there is a research gap in developing a fast, simple, and stable MPPT algorithm for solar tree applications.

Numerous optimization algorithms are employed in energy management systems, including metaheuristic techniques like genetic algorithms, particle swarm optimization, and ant colony optimization. These algorithms can adapt to dynamic weather conditions and maximize energy production from solar panels. Recently metaheuristic optimization methods have been addressed in many works to solve complex problems [11–20]. The novel one is called the Horse herd optimization (HHO) algorithm inspired by horses' behavior. The authors in [16], introduce HHO for high-dimensional optimization problems with the lowest complexity and least computational cost. In [13], the author applies HHO for validating concrete composition. Feature selection problems utilize a binary version of HHO in [14]. HHO is employed with deep learning in Web page modeling problems [15]. For solving power flow problems multi-objective HHO is used [16]. The sizing problem of the hybrid system is solved by proposing the HHO algorithm [17]. Thermodynamic equilibrium problems are solved by applying Honey Badger and HHO algorithms [18]. To enhance the weight function of the neural network in genetic disorder prediction [19], wild HHO with modification is employed. The above-stated research works show that HHO is applied in many optimization problems but not in MPPT.

Cascaded converters are used to improve the overall efficiency of the PV power system since they are more efficient for applications requiring high power and have low transmission loss (I²R). This paper proposes the cascaded buck-boost converter architecture using the HHO method, which aids in predicting the ideal DC-DC converter duty ratio depending on solar irradiation. The Cascaded converter will buck and boost the desired voltage depending upon the Load by using the HHO algorithm through the Raspberry Pi Pico controller. Lower voltage output ripple, minimal switching loss, and quicker transient response are all benefits of cascaded converters [20,21]. Raspberry Pi PICO is a small computer that provides a flexible environment to develop complex problems [22,23]. There's limited research on implementing PICO for real-time data acquisition, control of MPPT algorithms, and communication with smart grids.

While existing research covers individual aspects of the proposed system, a clear gap exists in combining these elements for a real-world implementation. By addressing these gaps, this research can contribute significantly to the advancement of efficient and adaptable solar tree systems for urban energy harvesting. In this work, we propose a novel MPPT algorithm based on Horse Herd Optimization (HHO), a bio-inspired optimization technique that simulates the behavior of a herd of horses. HHO has the advantages of high exploration and exploitation capabilities, fast convergence, and robustness to local optima [24,25]. We implement the HHO-MPPT algorithm using Raspberry Pi Pico, a low-cost, high-performance microcontroller board with flexible digital interfaces that can communicate with the solar PV system and the DC-DC converter [26]. We use Raspberry Pi Pico to implement a simple and efficient HHO-MPPT algorithm that can adapt to changing environmental conditions and load requirements. Therefore, we claim that Raspberry Pi Pico-based HHO-MPPT is a novel and effective solution for solar tree systems.

The rest of the article is structured as follows: A description of the system is given in Section 2. The third Section seeks HHO and MPPT algorithms, and Sections 3 and 4 present the software and hardware results and conclusions, respectively.

2. System Model

Figures 1 and 2 show the circuit diagram and the entire system block. The system block comprised the solar tree, voltage sensor, driver circuit, Raspberry Pi Pico controller for implementing the HHO algorithm, and a PWM generator, a cascaded DC-DC buck-boost type converter, and a utility load. In this work, an artificial solar tree for power generation is designed. Because it can produce as much as 10% more power than conventional PV systems while using just 1% land. In this work, Solar Tree consists of three PV panels/modules.

Each panel includes 20 series connected solar cells. To create a PV string, three panels of 60 cells in series are combined and again.

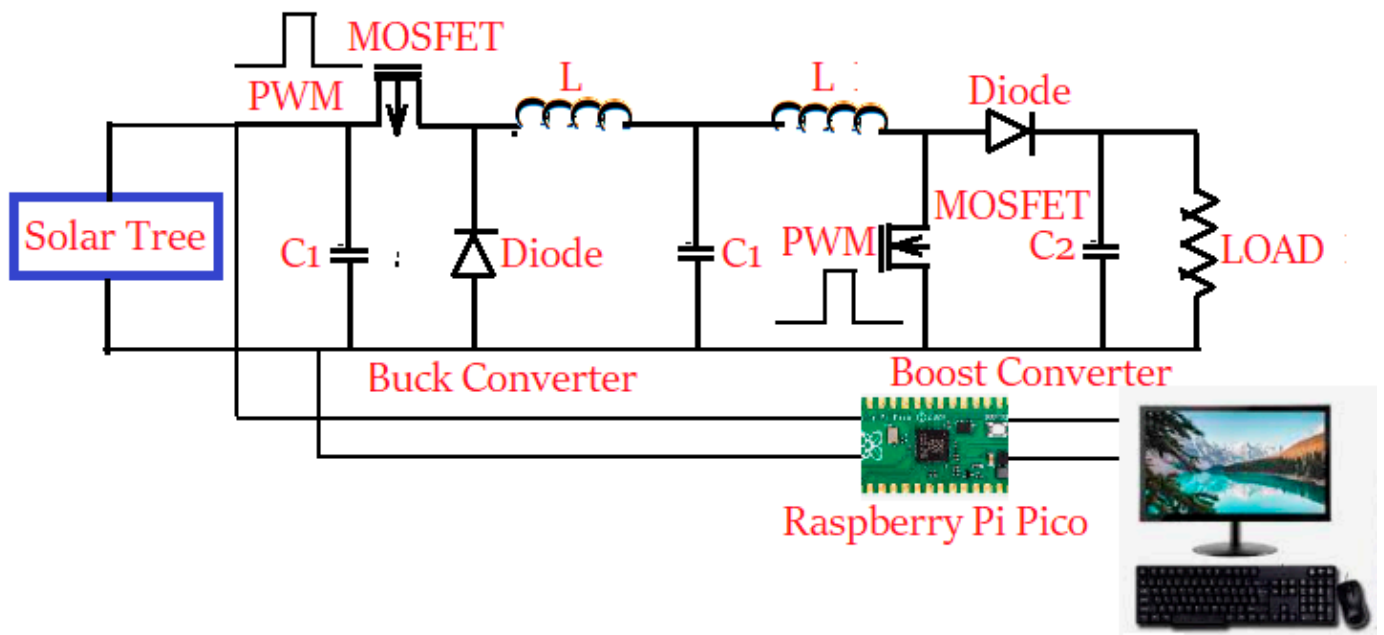


Figure 1. Circuit diagram.

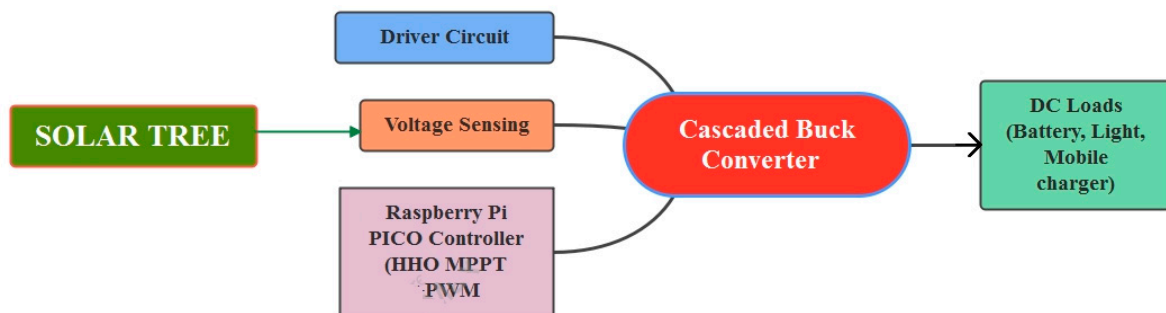


Figure 2. System block diagram.

The HHO algorithm is a new metaheuristic algorithm used to generate a duty cycle for the PWM generator. The PWM generator will generate a PWM signal for a cascaded DC-DC buck-boost converter. Load (light and mobile charger) is also connected next to utilized. Both the HHO algorithm and PWM generator are embedded in the Raspberry Pi Pico controller. A cascaded buck-boost controller is used in this work to run a constant DC load. Greater switching speed, simple fault isolation, less input current ripple, high efficiency, greater transient responsiveness by lowering electromagnetic emission and enhanced reliability are all benefits of cascaded converters over traditional buck-boost converters. The positive aspects of the Raspberry Pi Pico include affordability, portability, low power consumption, and suitability for real-time applications.

2.1. Solar Tree System

Natural tree-like structures were developed in this work while using less amount of land to generate maximum solar power output. Phyllotaxy refers to the positioning of leaves on a plant’s stem. It comes in three varieties: whorled, opposite, and alternate phyllotaxy. During alternating phyllotaxy, a single leaf emerges from a branch’s node. Two leaves grow from the node in opposite orientations on plants with opposite phyllotaxy. In plants with whorled phyllotaxy, the node produces three or more leaves. In this work solar

tree employs the previously mentioned alternate phyllotaxy pattern. Because the tree is made up of three panels that are 120 degrees apart from one another. Using this method has the advantage of preventing successive panels from shading one another and ensuring that each panel receives an equal amount of solar energy. The Fibonacci pattern is used to arrange the solar panels in a solar tree in a similar way to how leaves and branches are arranged in a real tree. The panels are arranged in different orientations to form the Golden angle, which is a fixed angle concerning each other. The Golden Ratio and Golden Angle in the Fibonacci Series are 1.618 and 137.5° , respectively. One can find the Golden ratio by dividing a Fibonacci number by the one that comes before it. Nearly 1.618 is the ratio.

$$\varphi = F_n / F_{n-1} = (1 + \sqrt{5}) / 2 = 1.6180339887 \dots$$

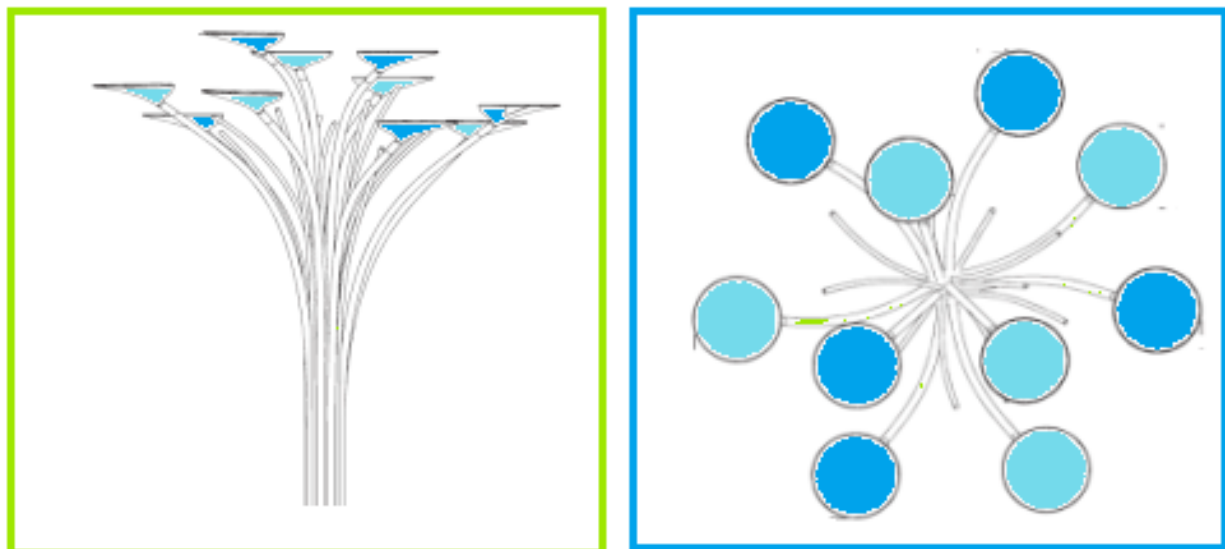
For example, $\varphi = 233 / 144 = 1.618$.

The smaller of the two angles formed by dividing a circle's circumference in half following the golden ratio is known as the "Golden Angle."

The Golden angle = $360^\circ \times F_n / F_{n+2} = 137.5^\circ$.

Using the above formula, the angle of any phyllotaxy pattern (1/3, 2/5, 3/8...) can be determined.

The designed system involves a solar panel of capacity 10 W. The detailed specifications are shown in Figure 2. High-quality, completely weatherproof 12 V, 10 W solar panel operates in both sunny and cloudy environments. The pipe length used in this case is 60" inches. For the 1/3 pattern, The Divergence Angle, $d = 360 \times 1/3 = 120^\circ$. The three different lengths of nodes required in the Fibonacci pattern. Hence the lengths $L_1 = 3''$, $L_2 = 5''$ and $L_3 = 8''$ used as stems which follow the Fibonacci series. The Standard Tilt Angle for North Direction is -30° and South Direction is $+30^\circ$. Each node has a constant distance of 6 inches. The Solar Tree base is designed rectangle with 1/4" L-Clamps for a Strong basement and is attachable using nuts & bolts for easy transportation are shown in Figure 3a,b. The flowchart in Figure 3b outlines the typical operation of a solar tree system.



(a)

Figure 3. Cont.

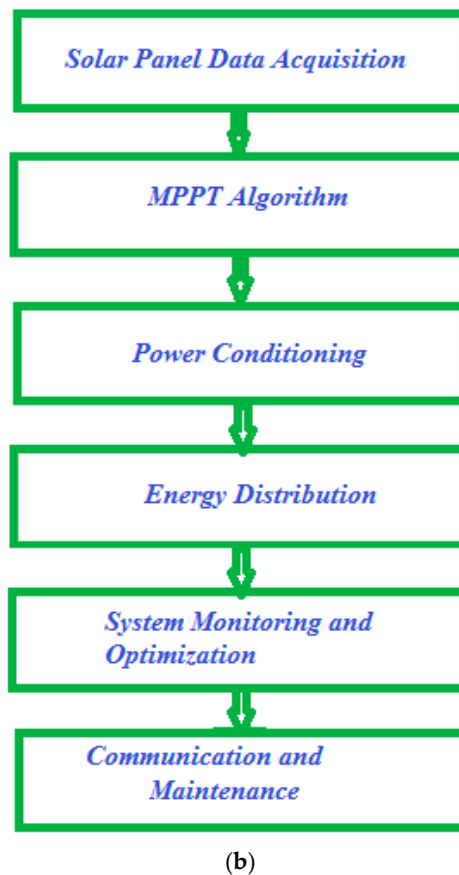


Figure 3. (a) Solar Tree front and top view; (b) Flowchart of Solar Tree.

2.2. Cascaded Buck-Boost Converter

A basic boost-buck converter depicted in Figure 4 changes a direct current voltage to a greater or lower direct current voltage. Reduced ripple currents in both the input and output circuits are further benefits of a cascaded converter. Higher efficiency is achieved by splitting the output current into two pathways, which significantly reduces I^2R and inductor losses.

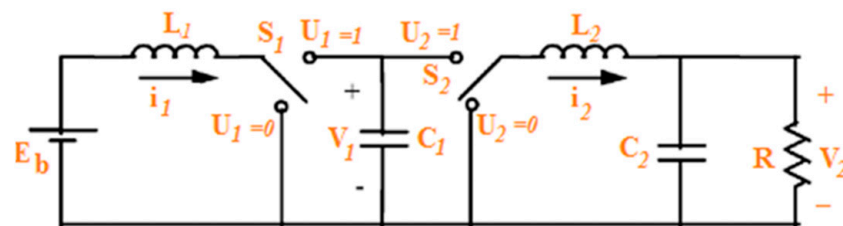


Figure 4. Cascaded buck-boost converter circuit diagram.

A Buck-Boost converter converts a positive direct current voltage at the input to a negative direct current voltage at the output. The equation for the output voltage of a cascaded buck-boost converter in terms of the input voltage and the duty cycles of the switches S_1 and S_2 is given by:

$$V_{out} = \frac{-D}{(1-D)} V_{in} \quad (1)$$

where D_1 and D_2 are the duty cycles of S_1 and S_2 , respectively. This equation can be derived by applying the principle of charge balance to the capacitors C_1 and C_2 and using the fact that the average voltages across the inductors L_1 and L_2 are zero. Energy is transmitted from the inductor to the capacitor, resulting in a decreasing inductor current

and an opposite polarity voltage across the resistor relative to V_{in} . Two IRF840 power MOSFETs are used in the cascaded buck-boost converter. One is for the buck side another for the boost. This is an N-channel type MOSFET, which can switch loads up to 500 V and 8 A. To drive a MOSFET, a driver circuit is designed that receives gate commands from Raspberry Pi Pico. Its switching speed is very high compared to the Arduino controller. Two separate power supplies are used for the driver circuit and converter circuit to avoid MOSFET saturation which leads to failure. To drive a MOSFET 12 V is required. But the Raspberry Pi Pico controller gives 3.3 V only. So to amplify the voltage, two separate TTL (Transistor–Transistor Logic) circuits are used for two MOSFETs. The driver circuit codings are written in Python using Thonny IDE. The Raspberry Pi Pico microcontroller, which plays a vital role in controlling the Cascaded converter producing constant switching frequency and variable duty cycle according to the HHO algorithm, is implemented.

2.3. Raspberry Pi Pico Controller

The Raspberry Pi Pico is an inexpensive microcontroller. It, like any other microcontroller, can be used to operate other electronic modules and sensors. Pico is breadboard compatible, with 40 GPIO pins working at 3.3 V (20 on each side) as shown in Figure 5. It is driven by a Dual-Core ARM Cortex M0+ processor. There are no headers on the 40 IO pins, however there are holes to simply solder headers. These 40 pins, as well as the three debug pins, have castellated edges. There are 26 IO pins and 14 power and system-related pins among the 40 pins. In addition to these 40 pins, there are three extra for (Serial Wire Debug) SWD Debugging.

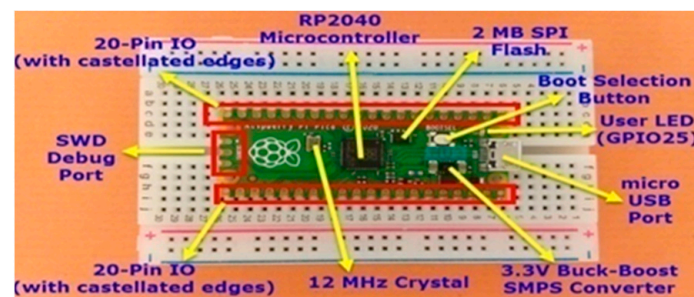


Figure 5. Board layout of Raspberry Pi Pico Controller.

2.4. Proposed Algorithm

As stated in the introduction section, MPPT is necessary for all solar PV plants to increase their efficiency. Our first and most significant task is to figure out which MPPT algorithm is optimal for the application. It is easy to implement conventional techniques like perturb and observe (P&O) and incremental conduction. However, it oscillates around MPP and struggles to adapt to changing environmental conditions. As a result, MPPT shifts to an algorithm based on machine learning (ML). Since ML yields positive results, data collecting is time-consuming, expensive to store data, and takes more effort to apply. In light of the literature review, this work planned to make use of optimization algorithms that already deliver positive outcomes in other disciplines. The chosen optimization algorithm in this research is the Horse Herd Optimization (HHO) algorithm which is further described in the sequential section.

HHO Method

Horse Herd Optimization (HHO) method was introduced in 2021. It is a population-based meta-heuristic approach for high-dimensional optimization problems that is mostly inspired by the behavior of horses being herded. HHO mimics the social behaviors of horses of various ages by utilizing six key features: grazing (G), hierarchy (H), sociability (S), imitation (I), defense mechanism (D), and roaming (R). Based on these behaviors, the HHO algorithm was developed. To find the optimal values of the algorithm's coefficients,

a sensitivity analysis is also carried out. Due to the numerous control factors that are based on the behavior of horses at various ages, HHO performs very well in resolving difficult issues in high dimensions. The suggested approach is compared to prominent nature-inspired optimization algorithms such as the grasshopper optimization algorithm (GOA), sine cosine algorithm (SCA), multi-verse optimizer (MVO), moth-flame optimizer (MFO), dragonfly algorithm (DA), and grey wolf optimizer (GWO). The proposed approach is extremely effective for high-dimensional global optimization issues, as demonstrated by the solutions of numerous high-dimensional benchmark functions (up to 10,000 dimensions). In terms of accuracy and efficiency with the lowest computational cost and complexity, the HHO algorithm likewise performs better than the aforementioned well-known optimization techniques. To choose features for high dimensional datasets, the Discrete Binary Horse Optimization Algorithm (DBHOA), a modified version of HHO, was used. Some bio-inspired algorithms perform better when exploring the search space, whereas others perform better when applied to the search space.

The authors applied novel Metaheuristic approaches to the HHO method for reproducing the MPPT with a solar panel. Here, the HHO approach is used to calculate the global MPP of PV systems under non-uniform illumination or partial shade, or the peak available MPP for uniform illumination.

The primary qualities of horses shown in Figure 6 are taken into account when developing the horse herd optimization algorithm.

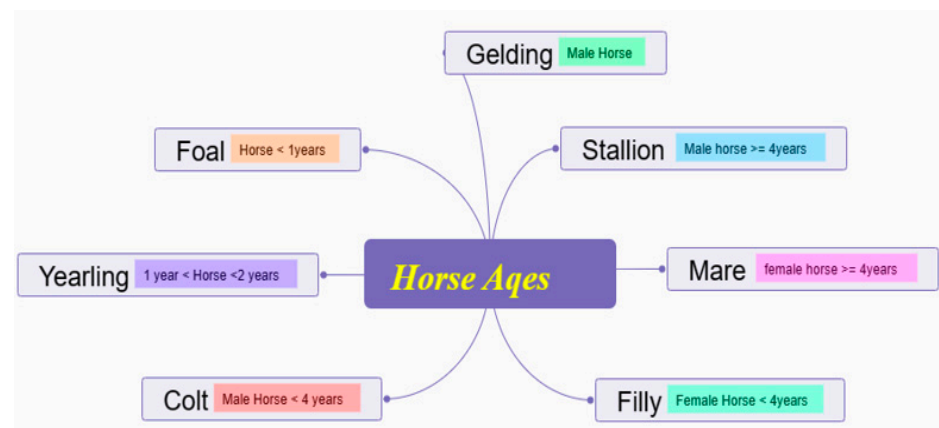


Figure 6. Characteristics of HHOA.

Mare (Female Horse)—Ruler—It leads the herd
 Stallion (Male Horse)—Protector—Keep herd members together
 Running is the horses' best form of defense.
 Due to their poor scores, some horses don't belong in the herd.
 Lifespan—25 to 30 Years
 Vision—360 °
 Brain weight—623 gm

Horses are classified as per the age they are

Delta (Age: Between 0–5)
 Gama (Age: Between 5–10)
 Beta (Age: Between 10–15)
 Alpha (Age: Older than 15)

Horses are relocated in response to Equation (2) on each iteration.

$$\vec{X}_m^{i,AGE} = V_m^{i,AGE} + X_m^{(i-1),AGE} \quad (2)$$

where,

X_i , AGE i th horse location,
 AGE horse age ($\alpha, \beta, \gamma, \delta$) range,
 I denote existing iterations, and
 $\rightarrow V_i$, AGE is the horse's velocity vector.

Horses behave differently depending on their age. A horse's lifespan can reach 25 to 30 years [19]. In this context, δ indicates horses that are between 0 and 5 years old, γ denotes that are between 5 and 10 years old, β reveals horses that are 10 and 15 old years, and also α shows above 15 years horses. In this work's optimization approach, the PV power is the goal function that must be maximized, while the duty cycle of the boost type converter is used as the optimization process variable. According to Equation (2), the particle's position (d_i) could be changed.

The velocity can be updated using Equation (3).

$$\begin{aligned} \rightarrow V_m^{\alpha} &= G_m^{\alpha} + D_m^{\alpha} \\ \rightarrow V_m^{\beta} &= G_m^{\beta} + H_m^{\beta} + S_m^{\beta} + D_m^{\beta} \\ \rightarrow V_m^{\gamma} &= G_m^{\gamma} + H_m^{\gamma} + S_m^{\gamma} + I_m^{\gamma} + D_m^{\gamma} + R_m^{\gamma} \\ \rightarrow V_m^{\delta} &= G_m^{\delta} + I_m^{\delta} + R_m^{\delta} \end{aligned} \quad (3)$$

Pasture/eating grass is mathematically represented in accordance with Equations (4) and (5).

$$\rightarrow G_m^{age} = g_i(\check{U} + p\check{l}) [X_m^{(i-1)}], age = \alpha, \beta, \gamma, \delta \quad (4)$$

$$g_m^{age} = g_m^{(i-1),age} \times \omega_g \quad (5)$$

where $\rightarrow G^{age}$ is the i th horse's motion variable,
 \check{l} & \check{U} are the pasture space's lower and upper boundaries, respectively, and P is between 0 and 1.

When they are of the 5 to 15 old years, the horses adhere to the rules of hierarchy [19]. It is characterized by Equations (6) and (7).

$$\rightarrow H_m^{age} = h_m^{age} [X_*^{(i-1)} - X_m^{(i-1)}], age = \alpha, \beta \text{ and} \quad (6)$$

$$h_m^{age} = h_m^{(i-1),age} \times \omega_h \quad (7)$$

where,

H^{age} illustrates how the optimum horse's position affects the velocity variable, and $X^{(i-1)}$ displays the optimum horse's position.

Factor S demonstrates that horses aged 5 to 15 become attracted to the herd that is expressed in Equations (8) and (9):

$$\rightarrow S_m^{age} = S_m^{age} \left[\left(\frac{1}{N} \sum_{j=1}^N X_j^{(i-1)} \right) - X_m^{(i-1)} \right], age = \beta, \gamma \quad (8)$$

$$s_m^{age} = s_m^{(i-1),age} \times \omega_s \quad (9)$$

where, S_m^{age} displays i th horse's social mobility vector and is also shows in the i th iteration the direction of the concerned horse approaches the herd.

In every cycle, S_m^{age} declined by the factor of ω_s .

N displays the overall number of horses.

The sensitivity analysis of the variables is employed to determine the coefficients S for β horse as well as γ horse. In the Equations (10) and (11) described the mimics behavior of horse.

$$\vec{I}_m^{i, age} = i_m^{i, age} \left[\left(\frac{1}{pN} \sum_{j=1}^{pN} \hat{X}_j^{(i-1)} \right) - X^{(i-1)} \right], age = \gamma \quad (10)$$

$$i_m^{i, age} = i_m^{(i-1), age} \times \omega_i \quad (11)$$

In Equations (10) and (11),

$\vec{I}_m^{i, age}$ is the i th horse's motion vector with \hat{X} locations.

pN displays the greatest-located horse.

The suggested value for p is horses of 10%.

In every cycle ω_i is the declined factor of i

Equations (12) and (13) illustrate the horses' defensive mechanism, which serves to prevent the horse from being in the wrong positions.

$$\vec{D}_m^{i, age} = -d_m^{i, age} \left[\left(\frac{1}{qN} \sum_{j=1}^{qN} \check{X}_j^{(i-1)} \right) - X^{(i-1)} \right], age = \alpha, \beta \text{ and } \gamma \quad (12)$$

$$d_m^{i, age} = d_m^{(i-1), age} \times \omega_d \quad (13)$$

where $\vec{D}_m^{i, age}$ is the i th horse's escape vector are given by vector \check{X} .

Moreover, qN displays the horses in the poor rest spots. It has been proposed that q is 20% of all the horses.

In every cycle, d^i declines the factor of ω_d .

A factor r simulates this wandering tendency and presents it as random movement. Baby horses nearly always exhibit roaming, which eventually decreases as they mature. Equations (14) and (15) depicts the process.

$$\vec{R}_m^{i, age} = r_m^{i, age} p X^{(i-1)}, age = \gamma, \delta \quad (14)$$

$$r_m^{i, age} = r_m^{(i-1), age} \times \omega_r \quad (15)$$

where, $\vec{R}_m^{i, age}$ is i th horse's random velocity

In every cycle $r_m^{i, age}$ declines the factor of ω_r .

Equations (4)–(15) are substituted into Equation (3) to generate the velocity vector.

The HHO algorithm gets the voltage and current of the solar tree as its input variables. The current power is calculated from these variables. In this algorithm, the right variables (maximum power) for the search must be picked. If the current power of the i th iterated horse is larger than the former fitness value, set it as current power. Secondly, choose the horse with the greatest overall power to be the global best. After evaluating each horse, each horse's location and speed can be changed while putting Equations (3) and (4) into consideration. When the ultimate goal is reached, the HHO outputs the ideal duty cycle and the optimum voltage corresponds to the global maximum power. Figure 7 presents the optimization procedure of the HHO algorithm.

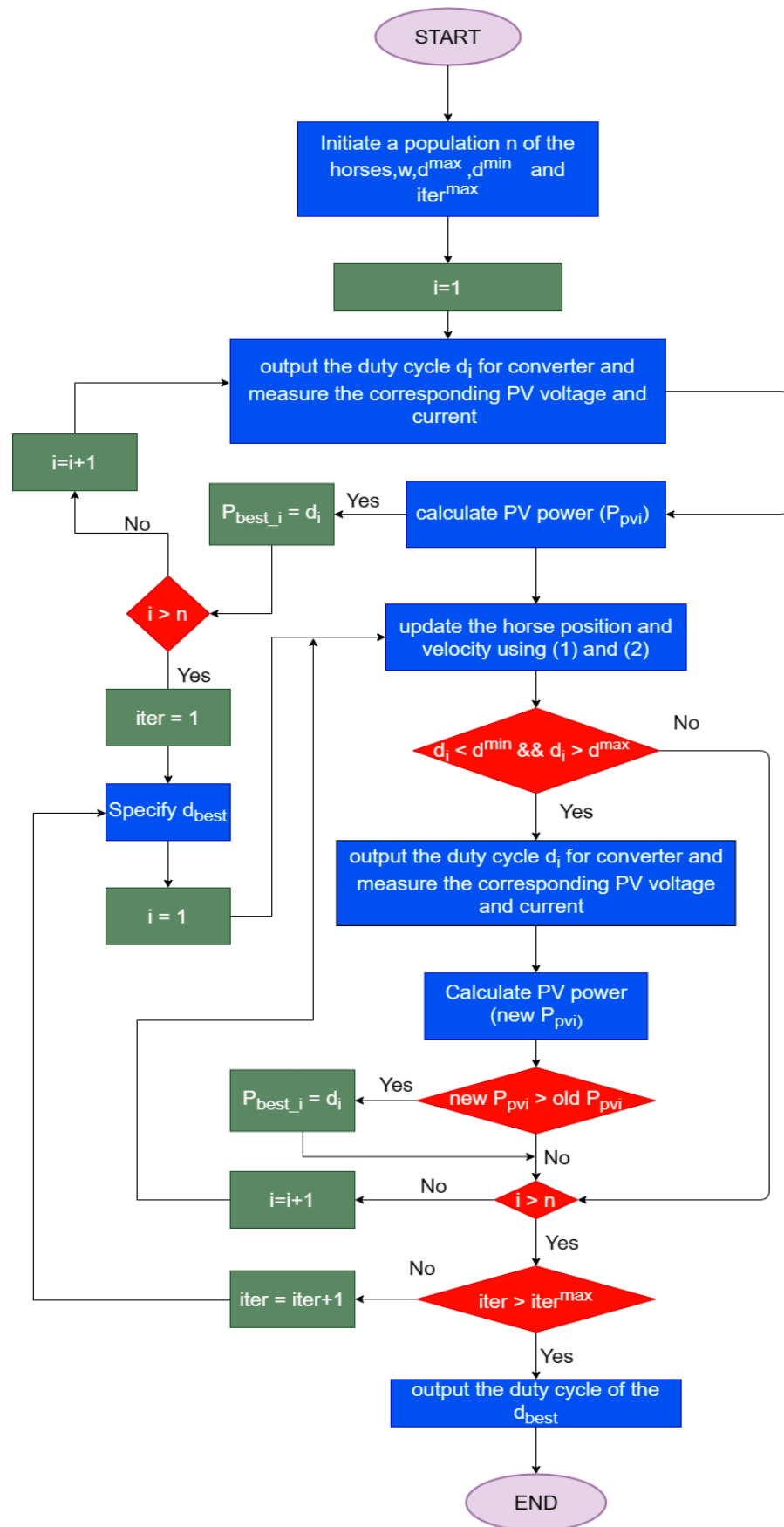


Figure 7. Flowchart of HHOA.

3. Results

3.1. Simulation Results

Since, the proposed system utilized three solar panels, the characteristics of panels in series and parallel connected are investigated and are depicted in Figures 8 and 9 and its parameters are tabulated nearby.

Solar Panel Datasheet			
Standart Test Condition (STC)			
3 Series			
Peak power	P	30	W
Open circuit voltage	Voc	63	V
Short circuit current	Isc	0.61	A
Maximum power voltage	Vmpp	54	V
Maximum power current	Impp	0.56	A

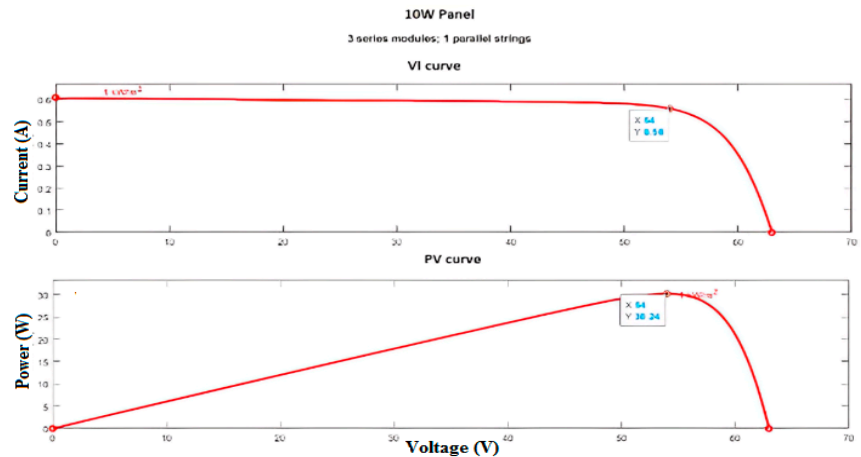


Figure 8. Characteristics curves of three Solar panels connected in series.

Solar Panel Datasheet			
Standart Test Condition (STC)			
3 Parallel			
Peak power	P	30	W
Open circuit voltage	Voc	21	V
Short circuit current	Isc	1.83	A
Maximum power voltage	Vmpp	18	V
Maximum power current	Impp	1.68	A

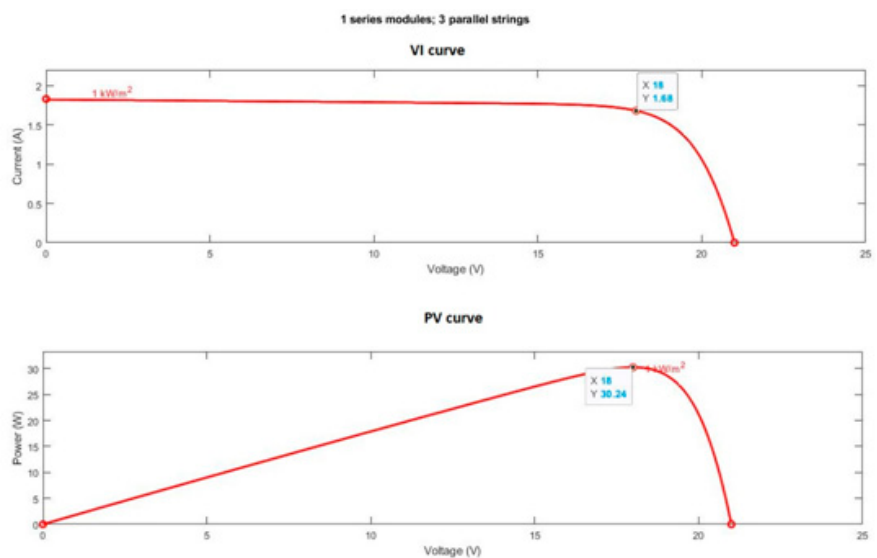


Figure 9. Characteristics curves of three Solar panels connected in parallel.

Three different cases are studied in MATLAB simulation to analyze the proposed horse herd optimization algorithm.

Case 1. Uniform irradiation condition

The P-V and I-V characteristics curve of uniform irradiation with maximum peak current and peak power denoted in red dot is shown in Figure 10. The cascaded buck-boost type converter's current in output, as well as input, its corresponding voltage, and power waveforms for the same irradiation condition (1000 W/m²), are shown in Figures 11–14. The converter's voltage on the output side was reduced from 59 V to 30 V to obtain the optimum value of 30 V. To maintain its power value of 250 W (three modules of 83.282 W × 3 = 249.846 W), the output current will be increased from 4 A to 8 A.

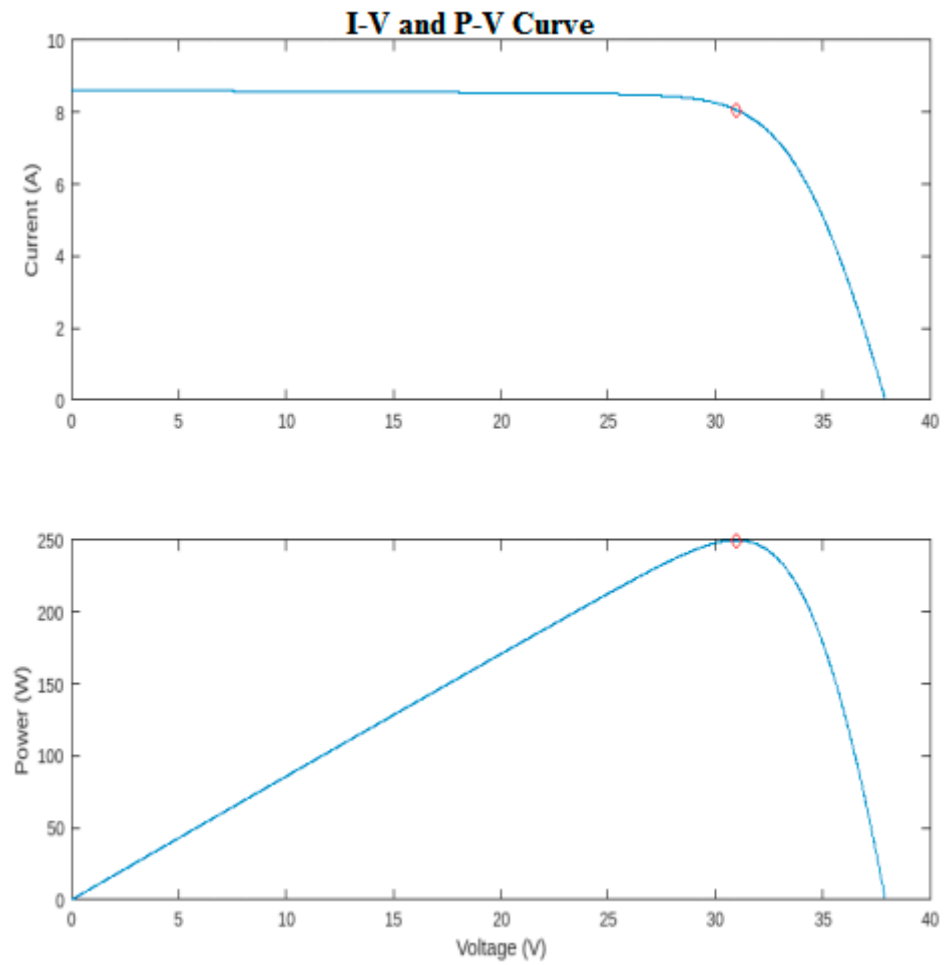


Figure 10. Characteristics curve under uniform irradiation for all 3 PV modules.

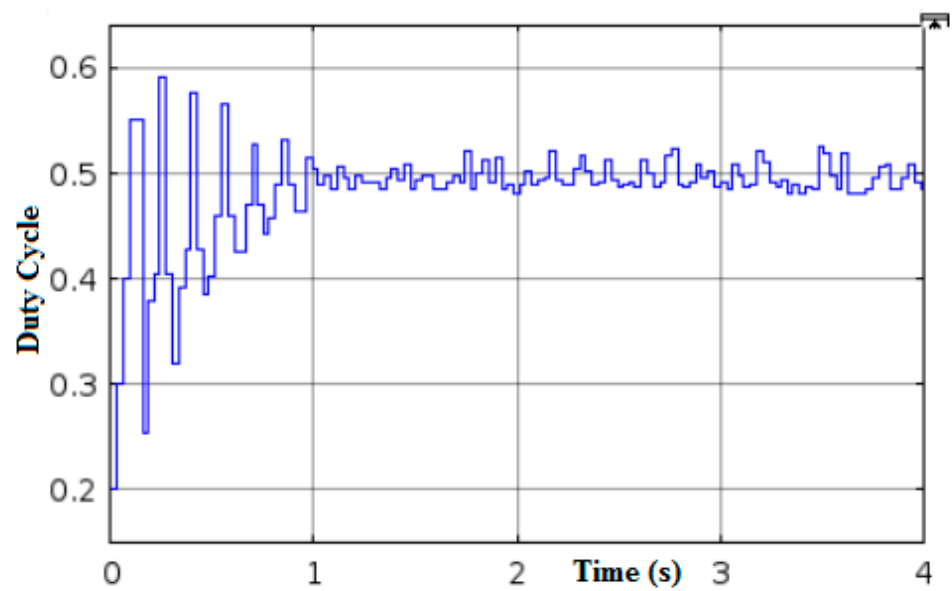


Figure 11. DC-DC boost converter's Duty cycle.

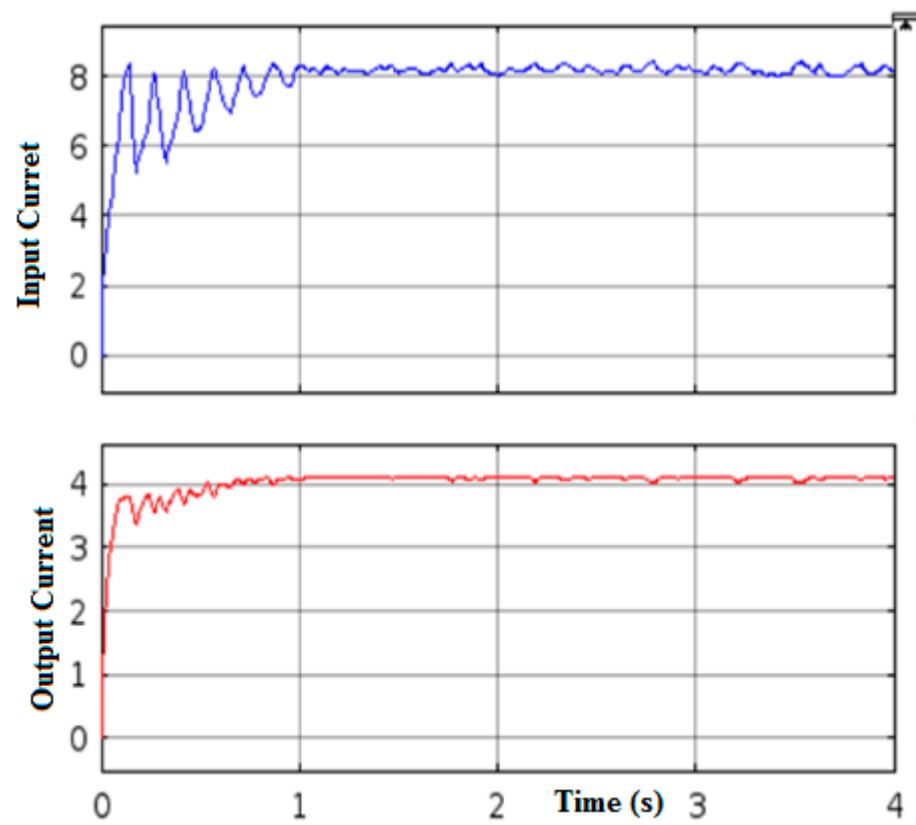


Figure 12. Converter's current waveforms—input side and output side.

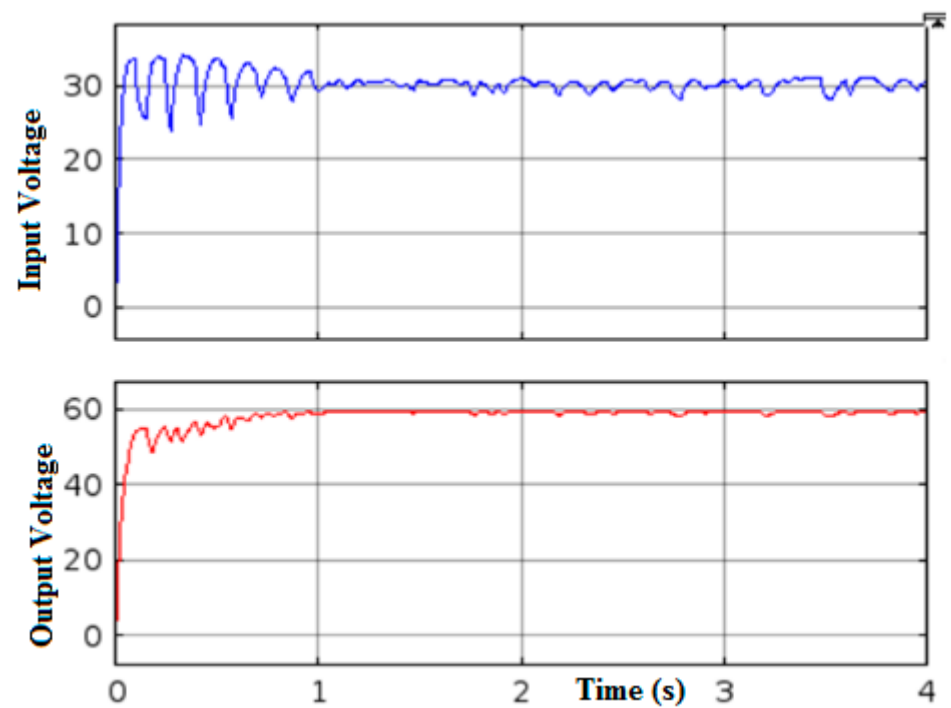


Figure 13. Converter's voltage waveforms—Input Side and Output Side.

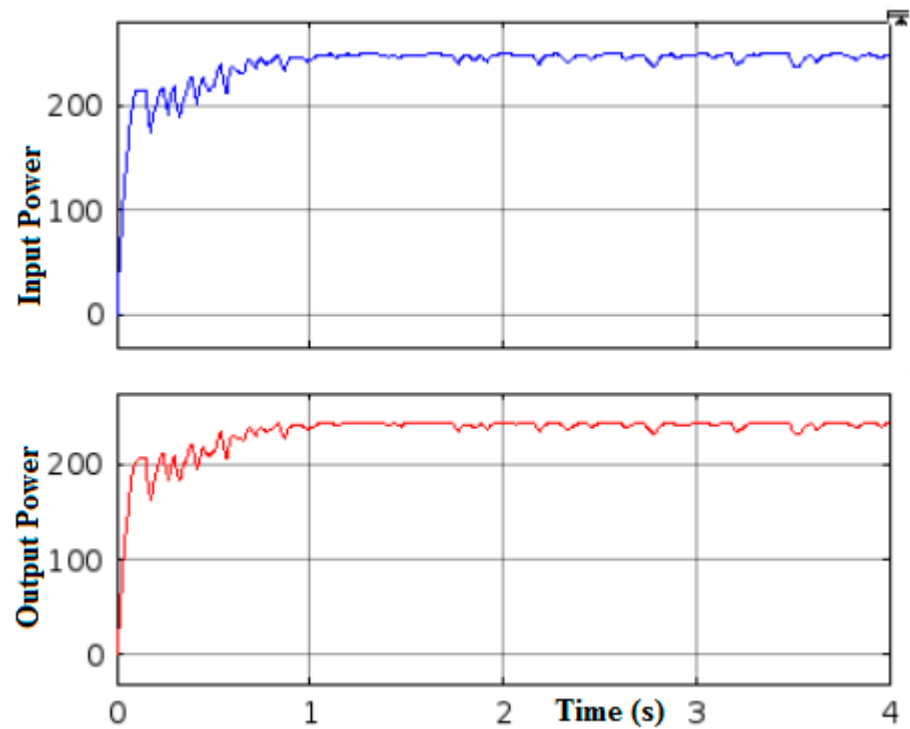


Figure 14. Converter's power waveforms—Input Side and Output Side.

Case 2. Non-Uniform irradiation condition

A PV module in a string is irradiated with 800 W/m^2 , to create non-uniform irradiation conditions. Figure 15 shows the non-uniform shading's characteristic curve with peak current and peak power denoted in red round. Based on the waveform, we can determine the maximum power (150 W) and its corresponding optimum voltage (20 V). The boost type converter's output side and input current, voltage, and power waveforms as well as duty cycle, are shown in Figures 16–19. Based on the waveform, we can infer that the converter's voltage dropped from 38 V of its input voltage to 20 V, which is its optimum value. As a result, the output current will increase from 3.21 A to 8.02 A to maintain its power value of 150.07 W.

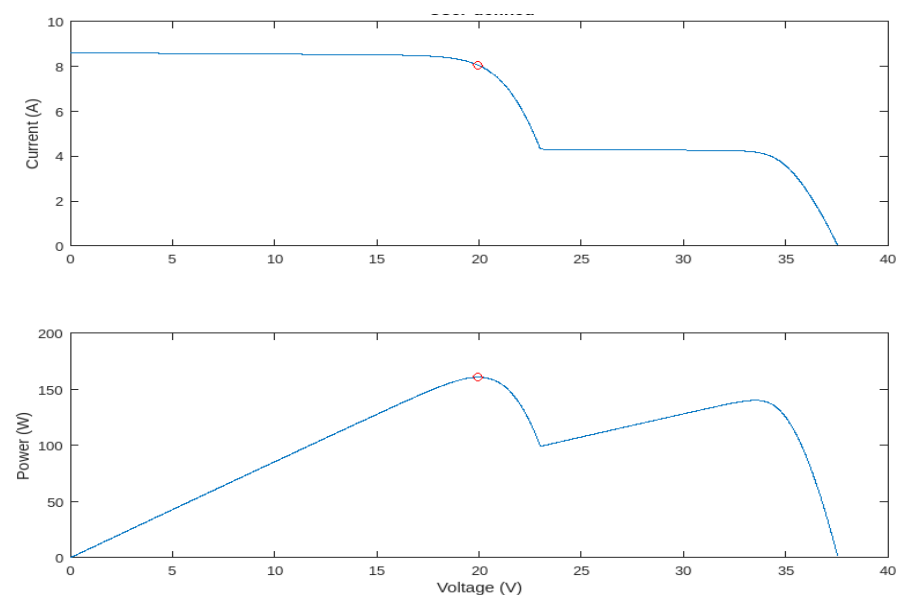


Figure 15. Solar Panel's Characteristics Curves under partial shading.

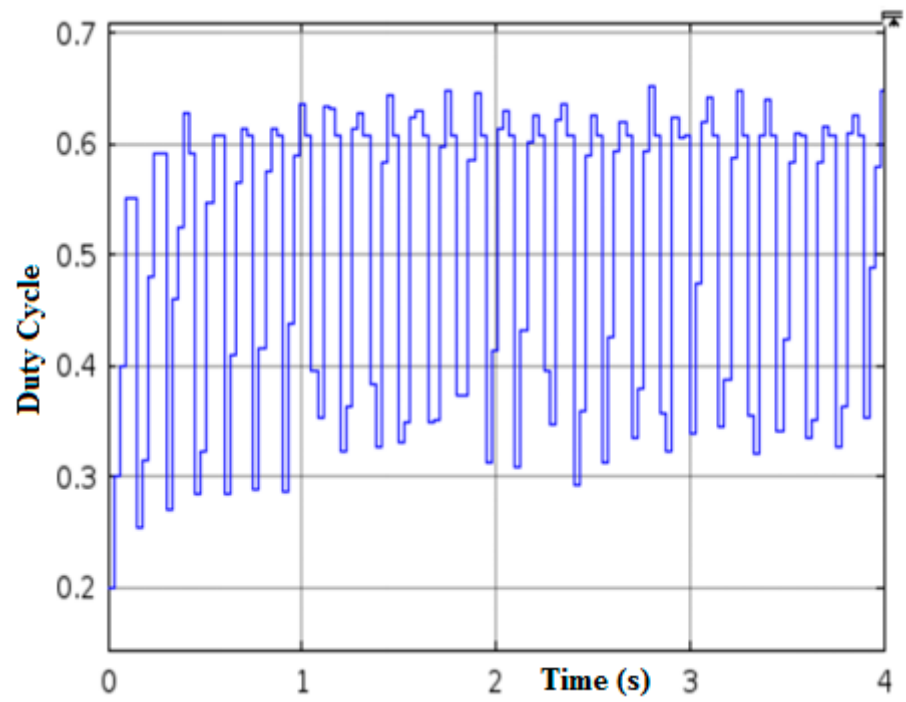


Figure 16. Duty cycle of converter.

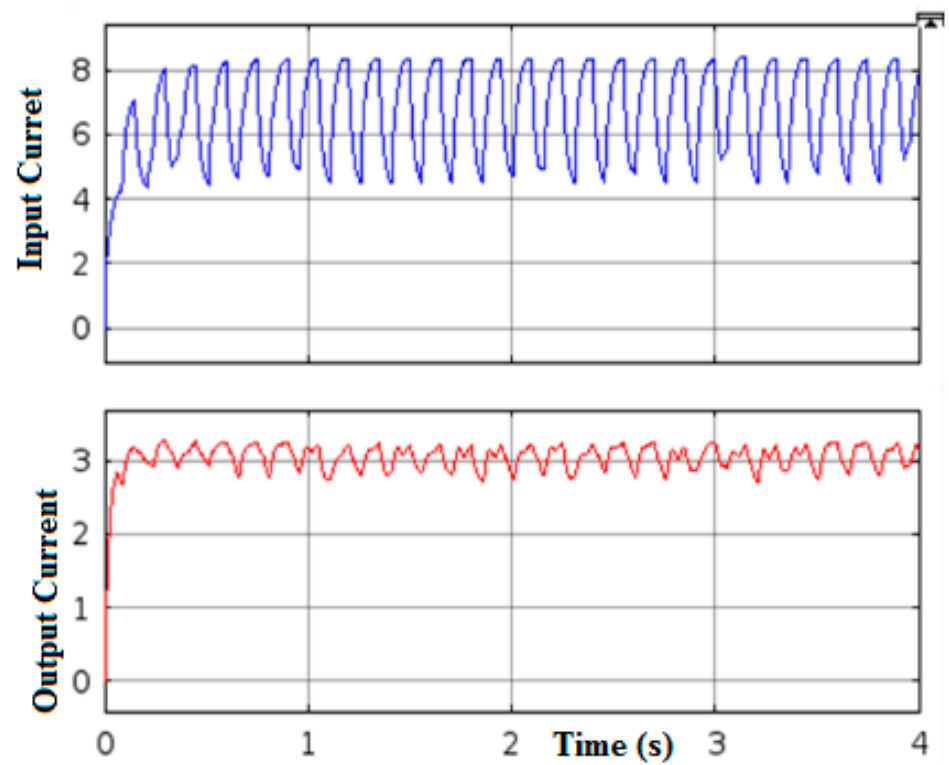


Figure 17. Converter's Current waveforms—Output side and input side.

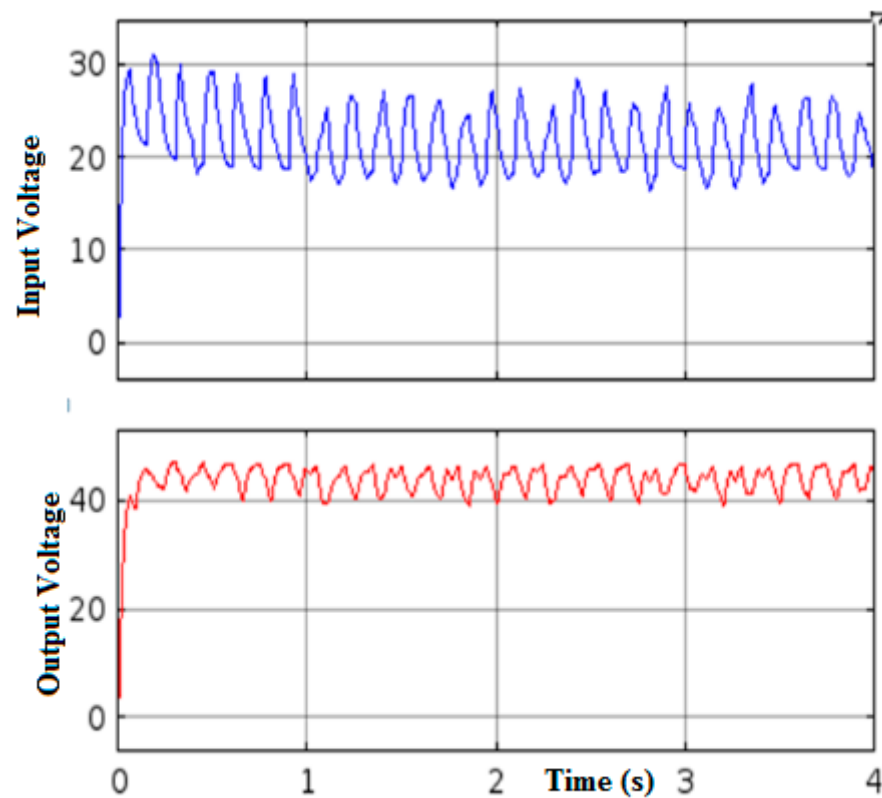


Figure 18. Converter's Voltage waveforms—Output side and input side.

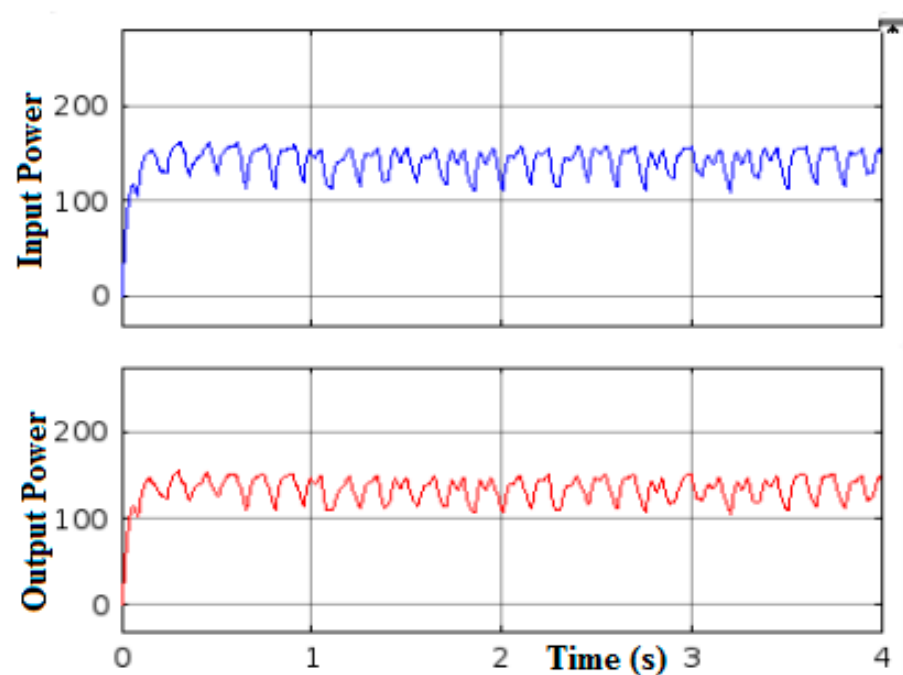


Figure 19. Converter's Power waveforms—Output side and input side.

Case 3. Non-uniform irradiation with 3 peaks

To generate non-uniform irradiation situations with three peaks, we apply 1000 Watt/m² through 500 Watt/m² irradiance towards the PV modules respectively. The curve under non-uniform irradiation with three peaks and global peak current and peak power denoted in red circles are depicted in Figure 20, which indicates that the global peak is 140 W and

its corresponding voltage value is 33 V. It is also able to be visible from the curve that there are two local maxima (73 W and 137 W) and global maxima (140 W). Below this situation, the duty cycle, output, and input parameters of I, V, and P waveforms of a boost type are depicted in Figures 21–24. Through analyzing the proposed algorithm's waveform, it's far evident that the converter's voltage (V) is an optimum voltage correctly tracked and has decreased from its input voltage value of 33.01 V to 40.11 V as its output. To hold its power of 140.01 W, the output current may be expanded from 3.32 A to 4.24 A.

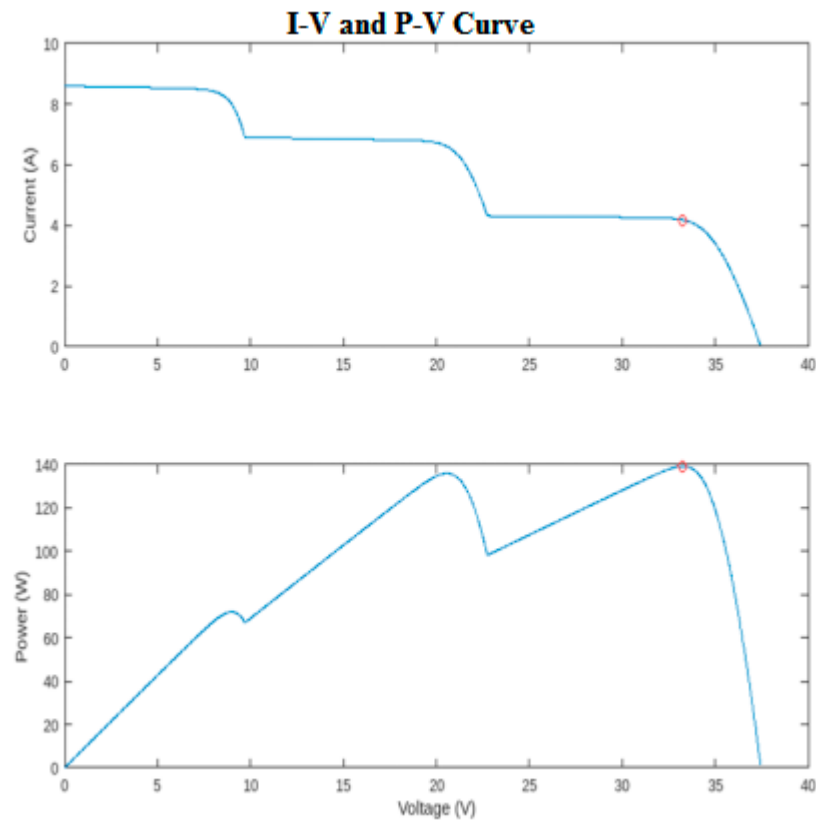


Figure 20. Characteristics Waveforms of solar panel under partial shading.

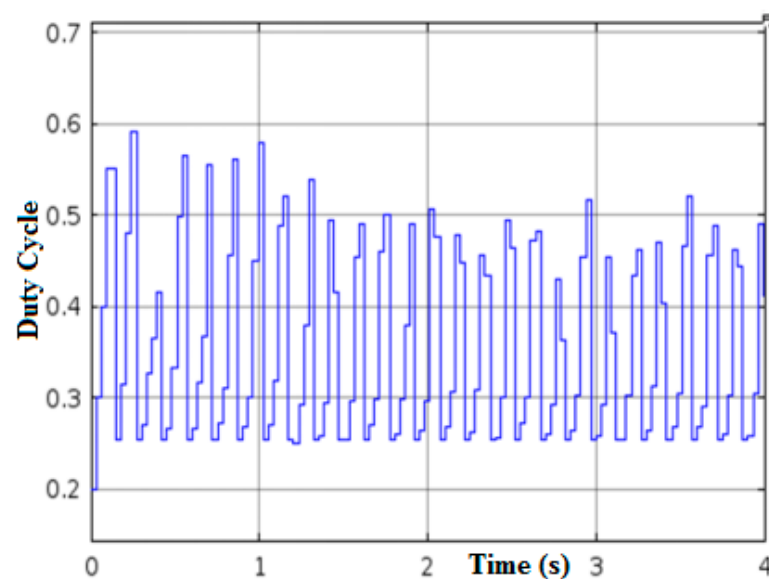


Figure 21. Duty cycle of converter.

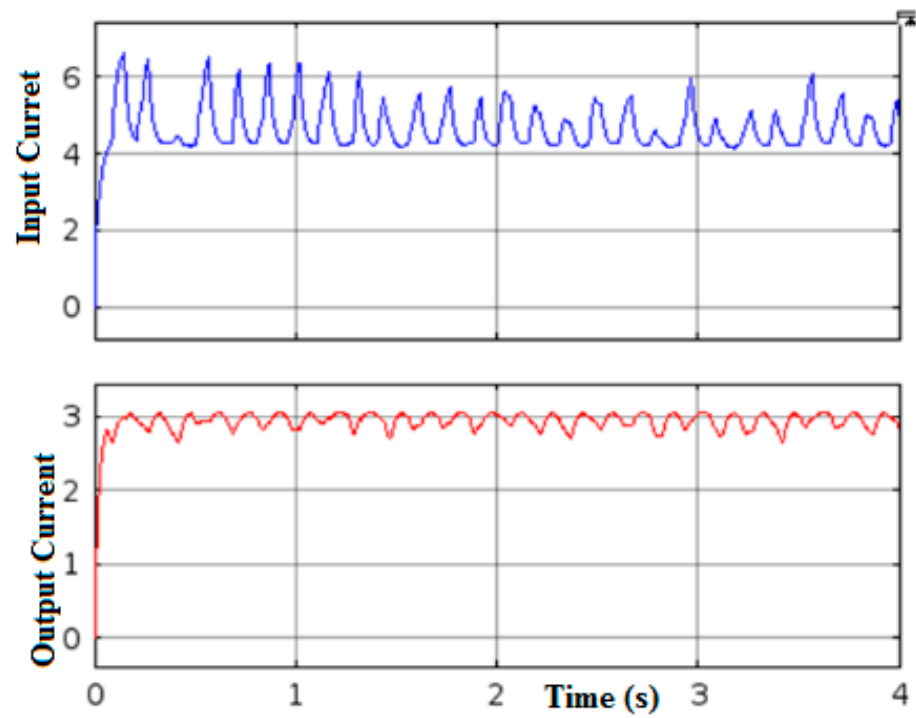


Figure 22. Converter's Current waveforms—Output side and input side.

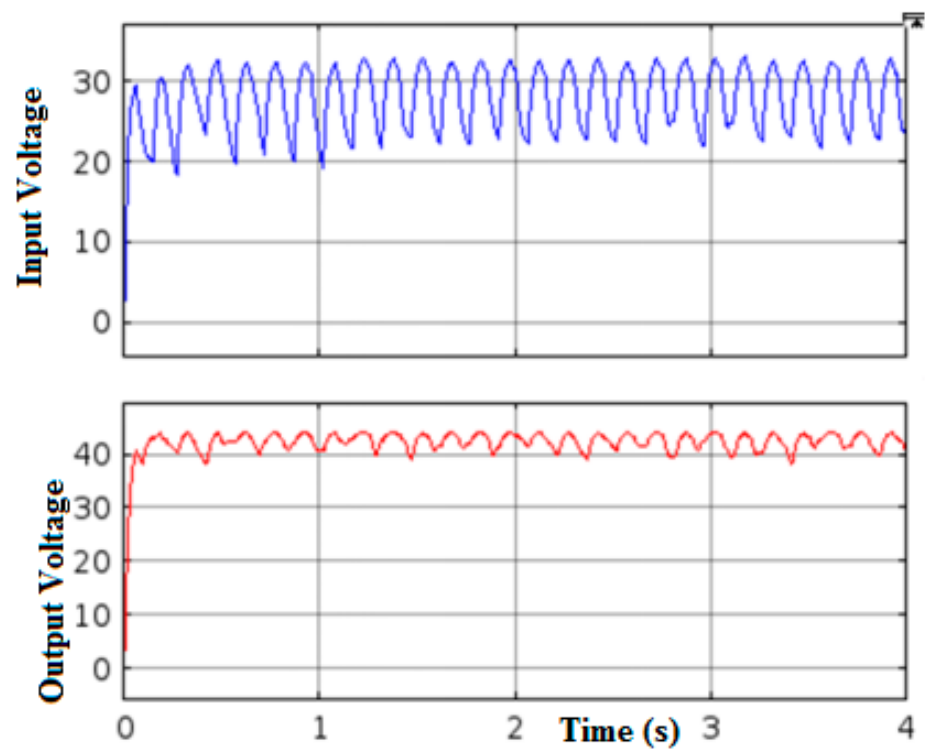


Figure 23. Converter's Voltage waveform—Output side and input side.

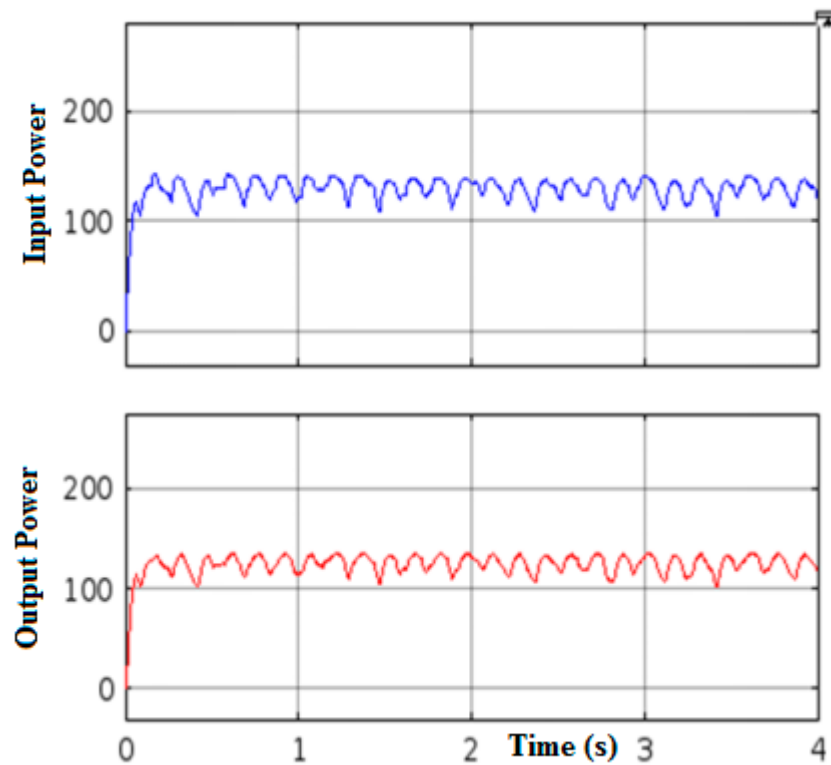


Figure 24. Converter's Power waveforms—Output side and input side.

3.2. Hardware Results

To get the results of the proposed system, it is required to design, test, and investigate each component used. Since the proposed prototype requires a current rating to drive load (light and mobile charger), the parallel connected solar panels are preferred to form solar trees. The solar tree is attached to the converter. The solar PV panel and its specification are depicted in Figure 25. This section discusses the design considerations and values of the converter's parameters which are tabulated in Table 1.



Figure 25. Converter's Power waveforms—Hardware setup.

Table 1. Cascaded Buck & Boost Converter Parameters.

S. No	Parameters	Theoretical Values
1.	Input voltage $V_{in}(avg)$	9.5 V
2.	Efficiency of the converter (η)	99%
3.	Buck Inductor (L_1)	0.78 H
4.	Boost Inductor (L_2)	564 μ H
5.	Buck Capacitor (C_1)	220 μ F
6.	Boost Capacitor (C_2)	22 μ F
7.	Switching frequency (F_S)	25 kHz
8.	Buck_Duty cycle ($D1$)	42.10%
9.	Boost_Duty cycle ($D2$)	20.83%
10.	Load resistance (R_L)	1000 Ω
11.	Ripple Voltage on Output side (ΔV_{out})	1.627 V
12.	Ripple current in Inductor (ΔI_L)	1.347 A
13.	Voltage on the Output side (V_{out})	12 V (Boost)
14.	Output voltage (V_{out})	4 V (Buck)

1. Input voltage ranges:

$$\text{Input side minimum Voltage } V_{in}(\min) = 8.0 \text{ V}$$

$$\text{Input side maximum Voltage } V_{in}(\max) = 11.0 \text{ V}$$

$$\text{Input side average Voltage } V_{in}(avg) = 9.5 \text{ V}$$

2. Output current & voltage ranges:

$$\text{Output Voltage } V_o \text{ (Boost)} = 12.0 \text{ V}$$

$$\text{Output Voltage } V_o \text{ (Buck)} = 4.0 \text{ V}$$

$$\text{Output Current } I_o = 1.0 \text{ A}$$

3. Calculation of Duty Cycle (Boost):

$$\text{Duty Cycle } D1 = 1 - \frac{V_{in}(avg)}{V_{out}} = 20.83\%$$

4. Calculation of Duty Cycle (Buck):

$$\text{Duty Cycle } D2 = \frac{V_{out}}{V_{in}(avg)} = 42.10\%$$

5. Calculation of inductor(Boost):

$$\text{Inductance } L1 = \frac{D1(V_{out} - V_{in}(avg))}{F_S * \Delta I_{L1}} = 564 \mu\text{H}$$

6. Calculation of inductor (Buck):

$$\text{Inductance } L2 = \frac{D2(V_{out} - V_{in}(avg))}{F_S * \Delta I_{L2}} = 0.78 \text{ H}$$

7. Calculation of inductor ripples current (Boost):

$$\text{Inductor Ripple Current } \Delta I_{L1} = 20\% \text{ to } 40\% \text{ of } I_o = 0.03 \text{ A}$$

8. Calculation of inductor ripples current (Buck):

Inductor Ripple Current $\Delta I_{L2} = 20\%$ to 40% of $I_o = 0.118$ mA

9. Output Capacitor selection (Boost):

$$\text{Output Capacitance } C_O = \left[\frac{I_o \cdot D_1}{F_s \cdot \Delta V_{\text{out}}} \right] = 22 \mu\text{F}$$

where,

$$\text{Output voltage ripple } \Delta V_{\text{out}} = ESR \left[\frac{I_o}{1-D_1} + \frac{\Delta L_L}{2} \right] = 0.378 \text{ V}$$

The toroidal core is used in the design of the cascaded buck-boost converter and Bobbin E type core inductor value of $564 \mu\text{H}$, 0.8H with respective to output capacitor value of $22 \mu\text{F}$ and $220 \mu\text{F}$ and reverses blocking diodes. MOSFET switch IRF540 is chosen for the switching circuit and the gate pulses to the switch are given through Raspberry Pi Pico microcontroller unit operating at 25 kHz switching frequency through pull up & pull down resistor.

Four 12-bit SAR-based analog to digital converters are supported by the Raspberry Pi Pico. Three of the four analog channels can be utilized. The 4th analog channel is for the internal temperature sensor whose value can be read by ADC4 pin. Solar Tree's voltage and current values are read by Raspberry Pi Pico controller's ADC pins. The Pi controller is embedded with HHO as well as PWM programs. The HHO algorithm delivers the optimal duty cycle to the PWM algorithm, which in turn sends the corresponding PWM signal to the cascaded buck-boost converter. Hence, for charging 4 V and 8 V battery, the CRO Scope results of PWM waveforms were obtained by analyzing the cascaded buck-boost converter as depicted in Figure 26a,b. The promising results were obtained by analyzing the cascaded converter with respect to 4 V , and 8 V batteries with variable solar voltages encouraging results were obtained as shown in Table 2.

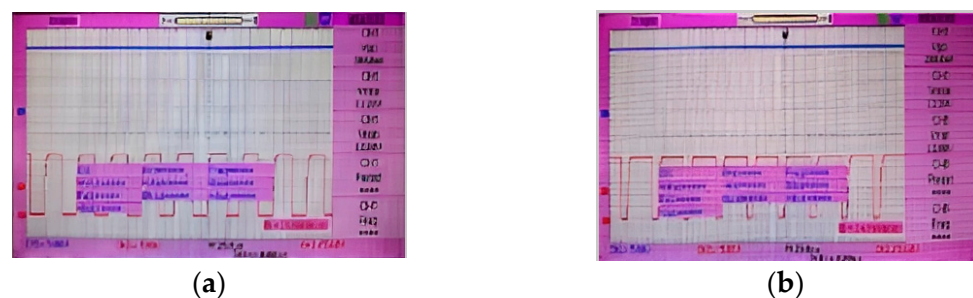


Figure 26. (a) Scope 4 V, (b) Scope 8 V.

Table 2. Input and Output tabulation for Battery System.

S. No	Input Voltage	Output Voltage	Cascaded Operation
	$V_{in}(avg)$	V_{out}	
	Variable Input	Constant Output	
1.	8.00 V	4.29 V	BUCK MODE
2.	8.49 V	4.33 V	
3.	9.08 V	4.30 V	
4.	9.58 V	3.86 V	
5.	10.01 V	4.26 V	
6.	10.41 V	3.87 V	
7.	11.07 V	4.93 V	
8.	11.94 V	4.17 V	

Table 2. Cont.

S. No	Input Voltage $V_{in}(avg)$	Output Voltage V_{out}	Cascaded Operation
	Variable Input	Constant Output	
9.	8.00 V	7.45 V	
10.	8.49 V	8.38 V	
11.	9.08 V	7.89 V	
12.	9.58 V	8.02 V	BUCK MODE
13.	10.01 V	8.07 V	
14.	10.41 V	8.15 V	
15.	11.07 V	8.17 V	
16.	11.94 V	8.15 V	
17.	8.00 V	15.80 V	
18.	8.49 V	16.02 V	
19.	9.08 V	16.04 V	
20.	9.58 V	16.07 V	BOOST MODE
21.	10.01 V	16.20 V	
22.	10.41 V	16.30 V	
23.	11.07 V	16.92 V	
24.	11.94 V	16.96 V	
25.	8.00 V	20.50 V	
26.	8.49 V	21.00 V	
27.	9.08 V	20.00 V	
28.	9.58 V	20.50 V	BOOST MODE
29.	10.01 V	20.00 V	
30.	10.41 V	20.50 V	
31.	11.07 V	20.00 V	
32.	11.94 V	20.50 V	
33.	8.00 V	24.30 V	
34.	8.49 V	25.20 V	
35.	9.08 V	23.60 V	
36.	9.58 V	25.00 V	BOOST MODE
37.	10.01 V	23.60 V	
38.	10.41 V	24.30 V	
39.	11.07 V	25.20 V	
40.	11.94 V	25.00 V	

Three panels are required for the development of a basic model of the phyllotaxy pattern in order to keep things simple. The specification of the solar panel is tabulated in Table 3. As a result, three 10 W panels totaling 30 W are chosen. It has been implemented A solar tree of three 10 W PV panels connected using a 1/3 spiral or alternate phyllotaxy pattern shown in Figure 25 and its PWM is shown in Figure 26a,b. Raspberry Pi GPIO pins can generate PWM signals based on the duty cycle. The hardware PWM output on the Raspberry Pi is connected to GPIO18 (P1–12). In this setup, the Raspberry Pi utilizes its GPIO pins to generate PWM signals, allowing for precise control over the duty cycle of

a square wave. This PWM output is facilitated by the hardware PWM capabilities of the Raspberry Pi, with GPIO18 (P1–12) specifically designated for this purpose. These PWM signals are then employed to regulate the power output of a cascaded buck-boost converter, a DC-DC converter capable of adjusting voltage levels as needed. The battery voltage dictates the PWM voltage levels generated by the Raspberry Pi, ensuring compatibility with the system’s requirements. This integrated control mechanism enables the Raspberry Pi to effectively manage and adjust the output voltage of the buck-boost converter, offering flexibility and efficiency in various applications. The cascaded buck-boost converter can be controlled using PWM signals from the Raspberry Pi. Depends upon the size of the battery voltage the Raspberry pi controller can generate PWM of 4 V or 8 V. The panels are connected with a cascaded buck-boost converter for obtaining maximum power from the solar panel which is controlled utilizing Raspberri pi pico controller. The separate driver circuit is designed for each MOSFETs as a switching device used for cascaded buck-boost converter. The entire setup of solar tree can be installed in public places like parks, gardens, hospitals, or schools with LED light and mobile charging facilities. In this study 12 W LED light is used who’s spectrum with wavelengths ranging from 380 nm to 940 nm. It enhances the beauty of the places as well as reduces the space occupied than common ground mounted solar panels.

Table 3. Solar Panel and its Specification.

S. No	Parameters	Rating
1	Maximum power	10.0 W
2	Open circuit voltage	21.6 V
3	Short circuit current	0.65 A
4	Maximum power voltage	19.6 V
5	Maximum power current	0.59 A

The comparison table of the optimal voltage and efficiency for each of the three test cases, as produced by the proposed HHO-MPPT algorithm, is shown in tabular form in Table 4. MPPT efficiency is a measure of how well a maximum power point tracking (MPPT) technique can extract the maximum power from a solar panel and deliver it to a battery or a load. MPPT efficiency can be calculated by dividing the output power of the MPPT by the input power of the solar panel, and multiplying by 100%. The formula is:

$$\text{MPPT efficiency} = (\text{Input power of solar panel} / \text{Output power of MPPT}) \times 100\%$$

I-V and P-V characteristic curves make it evident that, in general, without HHO-MPPT algorithm provided the voltage corresponds to the last/local maximum power point. A duty cycle offline was supplied by the proposed HHO-MPPT algorithm in MATLAB code to the Raspberry Pi PICO controller, which implements the PWM technique. The controller delivers optimal outcomes when it operates at an optimal duty cycle.

Table 4. Comparison Table.

S. No.	Test Cases	Optimum Voltage (V)		Efficiency (%)	
		With HHO-MPPT	Without HHO-MPPT	With HHO-MPPT	Without HHO-MPPT
1	Uniform irradiation condition	29.1	29.5	97.2	96.8
2	Non-uniform irradiation condition with 2 peaks	35.3	20.2	98.1	56.4
3	Non-uniform irradiation condition with 3 peaks	34.7	37.0	94.0	93.2

4. Conclusions

In this work, a novel metaheuristic optimization methodology of Horse Herd type implemented in a Raspberry Pi Pico controller is suggested to provide an offline duty cycle of cascaded buck-boost converter for solar tree application. Solar tree uses three panels connected using a spiral phyllotaxy pattern to prevent shading of other panels. Furthermore, solar tree structure decreases the land usage and increases the city's beauty. The cascaded buck-boost converter provides a duty cycle with fewer ripples in both input as well as output waveforms. Raspberry Pi Pico controller is an ultra-powerful dual-core, flexible microcontroller board with onboard flash memory that provides a duty cycle for a cascaded buck-boost converter. HHO algorithm is first simulated using MATLAB and a characteristics study is performed under three different cases where the proposed technique accurately identified the global maximum peak power value from other local peak values, which would be impossible without the specified algorithms. The results of our efficiency analysis show that our proposed MPPT technique can achieve the maximum power point (MPP) faster and more accurately. Since it provides outperformed results the same algorithm is validated using proto-type hardware and is compared with and without the proposed algorithm. From the results, it is recommended that MPPT use the same HHO metaheuristic optimization approach for future PV installations as well.

For future work, the work can be extended in the study to other types of solar tree systems, such as the ones with different geometries, orientations, and configurations. It is also intended to explore other optimization techniques that can improve the MPPT performance under dynamic and uncertain environments. Additionally, a smart MPPT system can be developed that can monitor and control the PV system remotely using the Internet of Things (IoT) technology.

Author Contributions: Conceptualization, K.P., A.S.R., R.S.S.N. and P.P.K.; Methodology, K.P., A.S.R., R.S.S.N. and S.R.A.; Software, K.P., A.S.R. and R.S.S.N.; Validation, K.P. and R.S.S.N.; Formal analysis, K.P., S.R.A. and M.F.I.; Investigation, S.A.S., S.R.A., P.P.K. and M.F.I.; Resources, S.R.A.; Data curation, P.P.K. and M.F.I.; Writing—original draft, K.P. and R.S.S.N.; Writing—review & editing, A.S.R., S.A.S., P.P.K. and M.F.I.; Supervision, S.A.S.; Project administration, A.R. and S.A.S.; Funding acquisition, A.R. All authors have read and agreed to the published version of the manuscript.

Funding: This research received no external funding.

Institutional Review Board Statement: Not applicable.

Informed Consent Statement: Not applicable.

Data Availability Statement: Data are contained within the article.

Conflicts of Interest: The authors declare no conflicts of interest.

References

1. Zuo, C.; Bolink, H.J.; Han, H.; Huang, J.; Cahen, D.; Ding, L. Advances in perovskite solar cells. *Adv. Sci.* **2016**, *3*, 1500324. [[CrossRef](#)]
2. Shariah, A.; Mahasneh, F. Emitter layer optimization in heterojunction bifacial silicon solar cells. *J. Semicond.* **2022**, *43*, 122701. [[CrossRef](#)]
3. Yang, Z.; Yong, P.; Xiang, M. Revisit power system dispatch: Concepts, models, and solutions. *iEnergy* **2023**, *2*, 43–62. [[CrossRef](#)]
4. Zhang, H.; Park, N.-G. Progress and issues in P-i-N type perovskite solar cells. *DeCarbon* **2024**, *3*, 100025. [[CrossRef](#)]
5. Walker, G.R.; Sernia, P.C. Cascaded DC-DC Converter Connection of Photovoltaic Modules. *Int. J. Power Control Comput. (IJPCSC)* **2013**, *5*, 34–41.
6. Chen, J.; Maksimovic, D.; Erickson, R. Buck-Boost PWM Converters Having Two Independently Controlled Switches. *IET Power Electron.* **2014**, *7*, 390–397.
7. Fu, J.; Zhang, B.; Qiu, D.; Xiao, W. A Novel Single-Switch Cascaded DC-DC Converter of Boost and Buck-Boost Converters. *IEEE Trans. Power Electron.* **2014**, *29*, 2807–2816.
8. Sheik Mohammed, S.; Devaraj, D. Design, Simulation and Analysis of Microcontroller based DC-DC Boost Converter using Proteus Design Suite. In Proceedings of the International Conference on Advances in Electrical & Electronics, AETAEE, Delhi, India, 28–29 December 2022; Elsevier: Amsterdam, The Netherlands, 2013.

9. Seetharaman, V.; Punitha, K.; Madavan, R.; Selvaganesh, V. Comparative analysis of PV based Cascaded Buck Boost converter for water pump applications. *Solid State Technol.* **2020**, *63*, 1–7.
10. Hariprasad, B.; Senthilkumar, R. Novel Design of VLT Cuk converter. *Int. J. Trends Eng. Technol.* **2015**, *7*, 66–71.
11. Geethanjali, M.N.; Sidram, M.H. Performance Evaluation and Hardware Implementation of MPPT based Photovoltaic System using DC-DC Converters. In Proceedings of the 2017 IEEE International Conference on Technological Advancements in Power and Energy (TAP Energy), Kollam, India, 21–23 December 2017.
12. Miaraeimi, F.; Azizyan, G.; Rashki, M. Horse herd optimization algorithm: A nature-inspired algorithm for high-dimensional optimization problems. *Knowl. Based Syst.* **2021**, *213*, 106711. [[CrossRef](#)]
13. Anjali, R.; Venkatesan, G. Optimization of mechanical properties and composition of M-sand and pet particle added concrete using hybrid deep neural network-horse herd optimization algorithm. *Constr. Build. Mater.* **2022**, *347*, 128334. [[CrossRef](#)]
14. Awadallah, M.A.; Hammouri, A.I.; Al-Betar, M.A.; Braik, M.S.; Elaziz, M.A. Binary Horse herd optimization algorithm with crossover operators for feature selection. *Comput. Biol. Med.* **2022**, *141*, 105152. [[CrossRef](#)]
15. Jayalakshmi, N.; Sangeeta, V.; Muttipati, A.S. Taylor Horse Herd Optimized Deep Fuzzy clustering and Laplace based K-nearest neighbor for web page recommendation. *Adv. Eng. Softw.* **2023**, *175*, 103351. [[CrossRef](#)]
16. Ida Evangeline, S.; Rathika, P. Wind farm incorporated optimal power flow solutions through multi-objective horse herd optimization with a novel constraint handling technique. *Expert Syst. Appl.* **2022**, *194*, 116544. [[CrossRef](#)]
17. Alanazi, A.; Alanazi, M.; ArabiNowdeh, S.; Abdelaziz, A.Y.; El-Shahat, A. An optimal sizing framework for autonomous photovoltaic/hydrokinetic/hydrogen energy system considering cost, reliability and forced outage rate using horse herd optimization. *Energy Rep.* **2022**, *8*, 7154–7175. [[CrossRef](#)]
18. Bamikole, J.O.; Narasigadu, C. Application of Pathfinder, Honey Badger, Red Fox and Horse Herd algorithms to phase equilibria and stability problems. *Fluid Phase Equilibria* **2023**, *566*, 113682. [[CrossRef](#)]
19. Nandhini, K.; Tamilpavai, G. Hybrid CNN-LSTM and modified wild horse herd Model-based prediction of genome sequences for genetic disorders. *Biomed. Signal Process. Control* **2022**, *78*, 103840. [[CrossRef](#)]
20. Mehrabi, N.; Pashaei, E. Application of Horse Herd Optimization Algorithm for medical problems. In Proceedings of the 2021 International Conference on INnovations in Intelligent SysTems and Applications (INISTA), Kocaeli, Turkey, 25–27 August 2021. [[CrossRef](#)]
21. Irudayaraj, G.C.R. Interconnection Efficiency in Grid-Connected Photovoltaic (PV) Systems Using Single-Phase Neural Network-Based Neutral Point Clamped and Cascaded H-Bridge Multilevel Inverters. *Int. J. Intell. Syst. Appl. Eng.* **2024**, *12*, 188–198.
22. Rizzo, S.A.; Scelba, G. ANN based MPPT method for rapidly variable shading conditions. *Appl. Energy* **2015**, *145*, 124–132. [[CrossRef](#)]
23. Hussaian Basha, C.; Palati, M.; Dhanamjayulu, C.; Muyeen, S.; Venkatareddy, P. A novel on design and implementation of hybrid MPPT controllers for solar PV systems under various partial shading conditions. *Sci. Rep.* **2024**, *14*, 1609. [[CrossRef](#)]
24. Madessa, H.B.; Shakerin, M.; Reinskau, E.H.; Rabani, M. Recent progress in the application of energy technologies in Large-Scale building Blocks: A State-of-the-Art review. *Energy Convers. Manag.* **2024**, *305*, 118210. [[CrossRef](#)]
25. Madhavi, J.; Emmadi, A. Sliding mode control PWM Converter. In Proceedings of the Power Electronics and Variable Speed Drives, Nottingham, UK, 23–25 September 1996; Conference Publication No. 429, IEE. 1996.
26. Gatla, V.R.; Injeti, S.K.; Kotte, S.; Polamarasetty, P.K.; Nuvvula, R.S.S.; Vardhan, A.S.S.; Singh, M.; Khan, B. An Effective Approach for Extracting the Parameters of Solar PV Models Using the Chaotic War Strategy Optimization Algorithm With Modified Newton Raphson Method. *IEEE J. Electron Devices Soc.* **2023**. [[CrossRef](#)]

Disclaimer/Publisher’s Note: The statements, opinions and data contained in all publications are solely those of the individual author(s) and contributor(s) and not of MDPI and/or the editor(s). MDPI and/or the editor(s) disclaim responsibility for any injury to people or property resulting from any ideas, methods, instructions or products referred to in the content.